

System-Level Calibration of a Millimeter-Wave Vector Signal Analyzer with Uncertainties

Joshua M. Kast, *Member, IEEE*, Paritosh Manurkar, *Member, IEEE*, Kate A. Remley, *Fellow, IEEE*, Dylan F. Williams, *Fellow, IEEE* and Robert D. Horansky, *Member, IEEE*

Abstract— We describe the system-level calibration of a vector signal analyzer operating at 28 GHz, including the determination of uncertainties in the magnitude and phase of measurements of a traceably characterized calibration waveform. We then apply the IEEE 1765-2022 measurement comparison approach to evaluate the uncertainty in error vector magnitude of the vector signal analyzer using an equivalent-time sampling oscilloscope with traceable calibration as the reference receiver. An additional measurement of the modulated waveform is made for comparison using a large-signal network analyzer operating on an arbitrary frequency grid, with good agreement to the sampling oscilloscope and vector signal analyzer in amplitude, phase, and error vector magnitude.

Index Terms—error vector magnitude; measurement uncertainty; vector signal analyzer; wireless system.

I. INTRODUCTION

IEEE-1765-2022 “Recommended Practice for Estimating the Uncertainty in Error Vector Magnitude of Measured Digitally Modulated Signals for Wireless Communications” [1] provides several methods to assess the contribution of a user’s receiver hardware and calibration to a measurement-based estimate of error vector magnitude (EVM) by comparison to EVM derived from a reference system. These methods require that the user first correct receiver impairments in a calibration step. The comparison then allows the user to assess the remaining receiver errors that were not corrected by the calibration and measurement process. Comparing nominal (computed) values of EVM and associated uncertainties allows the user to validate measurements and uncertainty analyses with respect to those made by a reference laboratory.

In this paper, we describe an implementation of the IEEE-1765-2022 Section 7.3: “Baseline EVM comparison of two receivers” measurement comparison with a vector signal analyzer (VSA) as the user receiver and an equivalent-time sampling oscilloscope as the reference receiver. A two-step process is illustrated (see Fig. 1) in which the user receiver is

first independently calibrated and then, in step 2, is brought to a reference laboratory to perform one of the IEEE-1765-2022 measurement comparisons. In our demonstration, one instrument, the sampling oscilloscope, is used to fulfill the roles of both the calibration- and reference receiver.

The sampling oscilloscope is an instrument of choice for traceable measurement of mmWave modulated waveforms due to its short traceability path with tractable uncertainty elements [2][3]. Specifically, the sampling oscilloscope’s architecture enables the transfer of phase calibration from a calibrated photodiode, that itself has been calibrated using an electro-optic sampling system (EOS) [4]. However, the sampling oscilloscope requires a repetitive waveform, a precise hardware triggering arrangement, and additional sinusoidal reference waveforms for correction of the sampling oscilloscope’s internal timebase [5]. Whereas previous studies have recognized the sampling oscilloscope’s utility for evaluating EVM as a reference instrument in the metrology-laboratory environment [6][7], the VSA is the tool of choice for practical and accurate measurement of waveforms from a variety of sources.

Calibration of vector receivers for step 1 is commonly carried out at the system level, although proprietary subsystem-level methods are also used by instrument manufacturers. For such system-level receiver calibrations, calibration coefficients correspond to the difference in the user-receiver measurement of a calibration waveform from those measured by a “calibration receiver” (a receiver that may be traceably calibrated to fundamental physical parameters). The magnitude and phase differences form the calibration coefficients, which provide an estimate the internal response of the user’s receiver. These calibration coefficients are then applied to future measurements of, for example, the IEEE-1765 Reference Waveforms.

There are two common approaches to system-level VSA calibration described in the literature. In one technique, a characterized pulse or comb generator forms creates a periodic waveform and serves as a phase transfer standard [8][9][10]. The comb generator is a wideband signal source which can be

traceably characterized in amplitude and phase [11] using an equivalent-time sampling oscilloscope. In [8], the broadband pulse from a comb generator is passed through a bandpass filter to produce a repetitive, band-limited calibration waveform. In recent research on real-time oscilloscopes [12], the electronic pulse generator is substituted by a photodiode, which has been directly characterized using an electro-optic sampling (EOS) technique [13].

A second class of technique makes use of modulated or multisine signals to calibrate vector receivers. Here, a modulated waveform is split by a power divider and measured simultaneously using a sampling oscilloscope and a VSA [14][15]. Sources of uncertainty include amplitude calibration, oscilloscope timebase distortion, and impedance mismatch. In some experiments, impairments are deliberately introduced into signals to provide a range of EVM values [16]. The IEEE-1765-2022 standard extends this technique by providing a library of Reference Waveforms with various classes of impairments [1]. A detailed overview on traceable measurement of modulated waveforms may be found in [18]. A recent study [19] uses a calibrated large-signal network analyzer (LSNA) to measure a modulated waveform transmitted from a signal generator to a receiver, and to verify the receiver’s EVM estimates.

For the calibration of vector receivers intended to measure EVM of modulated waveforms, we preferred the multisine-based approach, because repetitive multisine waveforms can more easily be tailored to emulate the statistical properties of our modulated waveforms of interest. Specifically, the peak-to-average power ratio (PAPR) of pulse waveforms is significantly higher than that of the typical modulated waveform.

Our work differs from other multisine-based VSA and EVM calibration efforts [14][15][16], wherein EVM was calculated using the VSA’s internal software, and the received waveform was not calibrated separately prior to EVM calculation. In contrast we treat the receiver calibration and EVM calculation as separate steps: first, the received waveform is calibrated in the frequency domain based on the VSA’s impulse response and impedance mismatch, then the EVM is calculated independently of the VSA’s internal software. EVM calculation and its accompanying steps (demodulation, matched-filtering, and equalization) are carried out using the IEEE-1765 algorithm. Meanwhile, receiver calibration is carried out independently of EVM, on the basis of linear corrections applied to the received signal in the frequency domain. Furthermore, we extend the work of [15] and [16] by applying a sequential technique for sampling-oscilloscope timebase corrections, which enables the direct measurement of arbitrarily-long waveforms using the sampling oscilloscope [17] – a necessary step to performing mmWave measurements. Notably, the key technical advances which enable the calibration described herein are the traceable calibration of the sampling oscilloscope [2][3][4][5][6][7], and the ability to extend sampling oscilloscope corrections to waveforms of arbitrary length [17], which together allow for the traceable measurement of communications signals directly at mmWave frequencies.

In Section II, we demonstrate the calibration technique on a VSA operating near 28 GHz. In Section III, we present results from a measurement-based estimate of EVM from a 64-QAM waveform, similar to the Reference Waveforms specified in IEEE-1765-2022. Uncertainties in amplitude, phase, and impedance mismatch are incorporated into the final EVM estimate. The uncalibrated VSA-derived EVM has a mean value over multiple repeat measurements of 3.22%, while the reference measurement has a mean value of 0.64%. After calibration, the VSA waveform measurement shows a reduction of 2.59% EVM to a mean value of 0.65%. As expected, this agrees well with the value from the reference receiver because the same sampling oscilloscope was used as both the calibration and reference receiver. These results were compared using the calibration-comparison methodology described in IEEE-1765-2022 Section 7.6, and the calibrated VSA measurements were found to agree with the reference-receiver measurements. As an additional demonstration of the technique, the test waveform was measured using an LSNA that had been calibrated in phase using the sampling oscilloscope calibration receiver. The measured EVM value of 0.67% in from the LSNA was also found to agree with the reference-receiver measurement using the calibration-comparison method of [1].

The VSA user receiver used in this demonstration was a Agilent N9030 PXA Signal Analyzer. This analyzer uses a heterodyne receiver architecture, wherein the incoming RF signal is optionally filtered and amplified, then downconverted

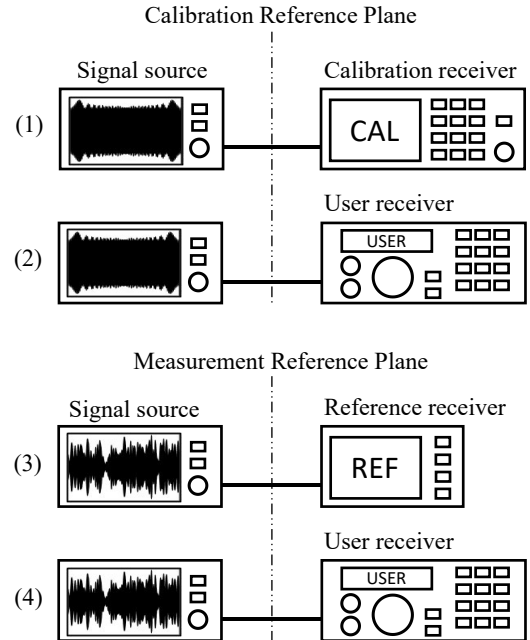


Fig. 1: Illustration of a system-level calibration procedure in an IEEE-1765 Measurement Comparison. Step (1), the calibration waveform is applied to the calibration receiver. Step (2), the same calibration waveform is applied to the user receiver at the same reference plane. In step (3), a reference receiver (generally different from the calibration receiver) measures a communications waveform. In step (4), the user receiver measures the same communications waveform at the same reference plane, and the two measurements are compared. Calibrations performed at the reference plane include S-parameter, power, and phase standards. The reference plane may be different between the calibration and reference laboratories.

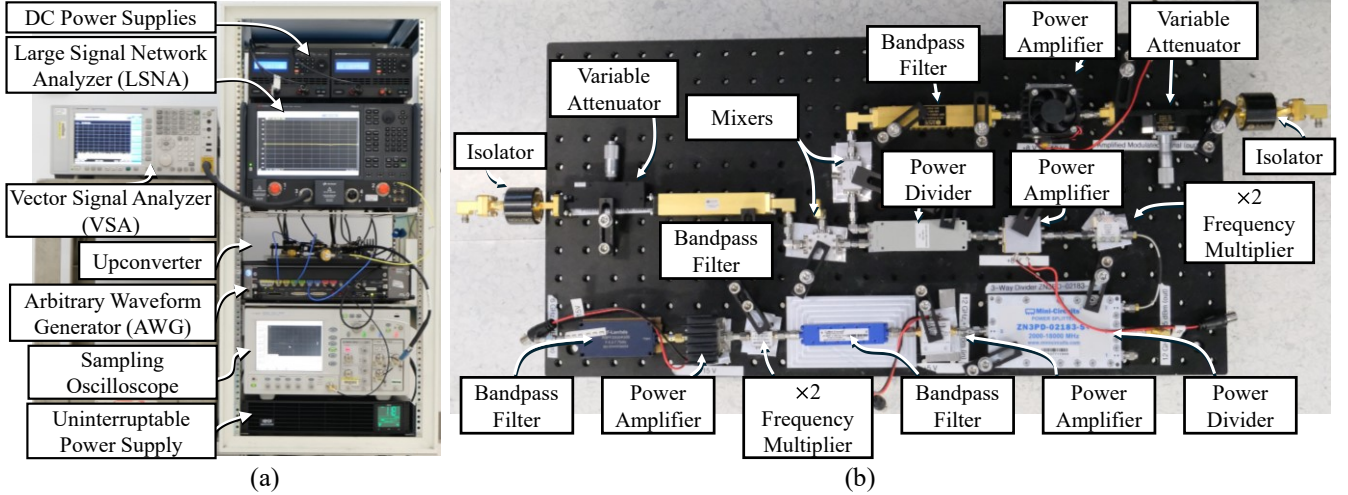


Fig. 2: Photographs of measurement setup. In (a), the instruments are configured for user-receiver (VSA) measurement, with the modulated signal output connected to the VSA input. The upconverter board, shown in (b), provides two independent 28 GHz modulated outputs, and one 12 GHz sine wave used for oscilloscope timebase correction.

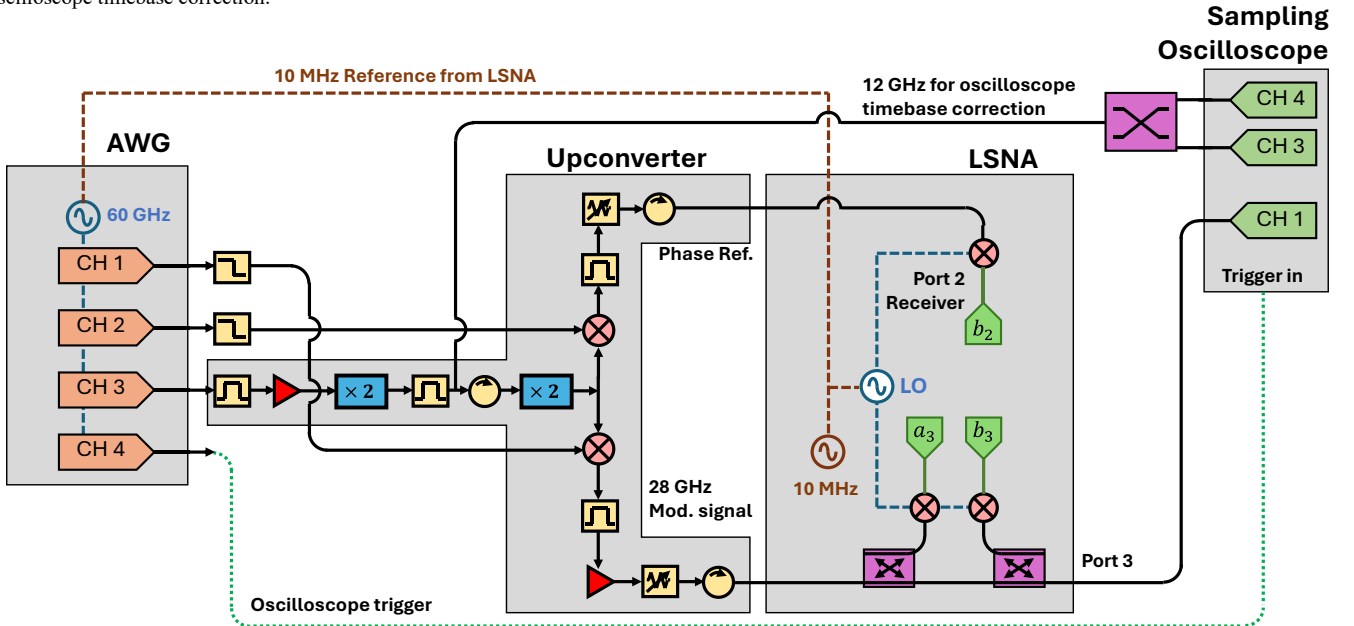


Fig. 3: Block diagram of measurement setup, shown with the reference receiver (sampling oscilloscope) attached. During user-receiver (VSA) measurements, the sampling scope is removed from the system, and the VSA attached to LSNA port 3.

to a single baseband channel, which is filtered and measured by an analog-to-digital converter. Within the PXA unit, the Keysight 89601B software records data from the receiver for display on the instrument’s screen. The 89601B software provides “Save Trace” function to save frequency-domain receiver data (complex Fourier coefficients) in Matlab (.mat) format for further analysis. We automate this function on our analyzer to allow 200 repeat VSA measurements to be collected in approximately 4 minutes. The VSA is not triggered by the incoming RF signal – instead, the 200 acquisitions are collected consecutively, and are time aligned in post processing. Different VSAs may require different procedures for saving waveform data, but the requirement for this calibration technique is that the data be saved as Fourier (complex) coefficients covering the bandwidth of interest.

While we demonstrate the method with a relatively narrowband VSA (160 MHz bandwidth), the method is

applicable to many user-receiver types including real-time or equivalent-time sampling oscilloscopes or other waveform recorders.

II. CALIBRATION OF THE USER RECEIVER

In the IEEE-1765 measurement comparison, the user receiver is first calibrated at the user’s lab by measuring its frequency-dependent impedance mismatch and impulse response using transfer standards such as a calibrated modulated-signal source (phase), calibrated power sensor (magnitude), and vector network analyzer (impedance). This process is illustrated in Fig. 1. We demonstrate this procedure by use of a modulated-signal source (which we term the “calibration source”) that generates a waveform (the “calibration waveform”). The calibration waveform that is emitted from the source has been characterized in phase, magnitude, and impedance mismatch by a calibration receiver

with a characterized impulse response and reflection coefficient. This calibration source is then used as a transfer standard to calibrate the user receiver. Photographs of the calibration source, reference receiver, and user receiver are shown in Fig. 2, and a block diagram of the system including 28 GHz upconverter is shown in Fig. 3. In our setup, an arbitrary waveform generator (AWG) generates baseband signals and a 6 GHz LO signal. This LO is multiplied to 24 GHz, and combined with 4 GHz IF waveforms to produce 28 GHz modulated waveforms, which can be connected to the user receiver (as shown in Fig. 2), or the reference receiver (as shown in Fig. 3). The upconverter also provides a 12 GHz output to the oscilloscope, which is used for timebase correction as described in [5]. Modulated signal measurements using the LSNA are described later in Section III.C, but the LSNA was present in the system at all times, as illustrated in Fig. 3. This choice was made to minimize changes in the setup between reference-receiver and LSNA measurements, as well as to allow impedance mismatch measurement of the user receiver. Note that it is possible to perform all parts of this calibration except the LSNA measurements described in Section III.C without inserting an LSNA into the modulated signal path.

In order to be an effective transfer standard, the source has been designed to provide a stable and repeatable output signal to within a desired uncertainty limit. The isolator placed at the source's output reduces the impact of changes in load impedance on the source's output signal (for example, if changes in load impedance affected the operation of the power amplifier). The upconverter portion of the source is attached to an optical breadboard to provide physical and thermal stability. Finally, many repeat oscilloscope measurements taken over a long time duration serve to capture any remaining noise or drift in the source, and allow us to account for these uncertainty elements in our overall uncertainty analysis.

A. Generation of the Calibration Waveform

The calibration waveform to be used should span at least the intended frequency range of the application of interest. When the calibration waveform is significantly wider in bandwidth than the modulated signal of interest, it is possible to characterize intermodulation and other out-of-band effects. Note that the calibration described herein does not correct for nonlinear properties of the receiver. Therefore, it is important to keep the receiver within its linear operating range during the waveform measurements. In order to do this, we adjust the signal power level and VSA gain to ensure that the applied signal amplitude is within the linear range of the VSA's digitizer. The calibration waveform must be periodic and use approximately the same frequency step as the waveform to be measured. The calibration waveform needs not transmit actual data and multisine signals [20][21][22] are often used.

To illustrate the calibration method, we used a 101-tone multisine signal as the calibration waveform for a mmWave-band VSA having a 160 MHz measurement bandwidth. While this VSA was not able to measure an IEEE-1765 Reference Waveform (which are typically 1 GHz bandwidth), the procedure illustrated here is identical, and the waveform we

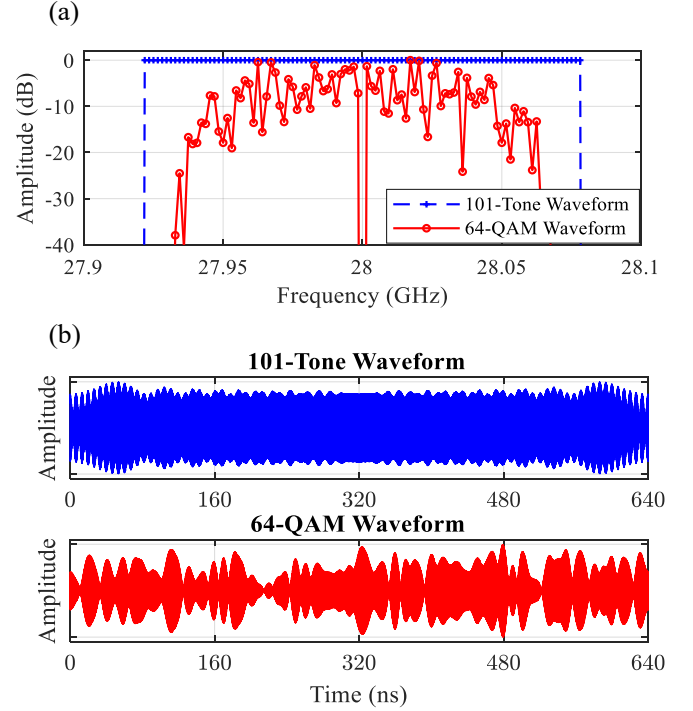


Fig. 4. (a) Frequency-domain and (b) time-domain plots of calibration waveform (101-tone) and 64-QAM modulated communications waveform.

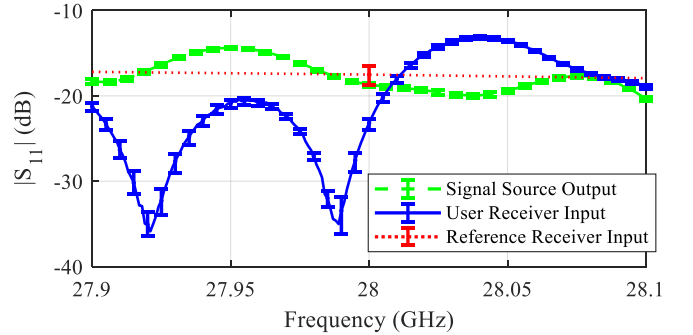


Fig. 5. Impedance mismatch (S_{11}) measurements for the calibration signal source and user receiver with uncertainties bounded by 95% confidence intervals.

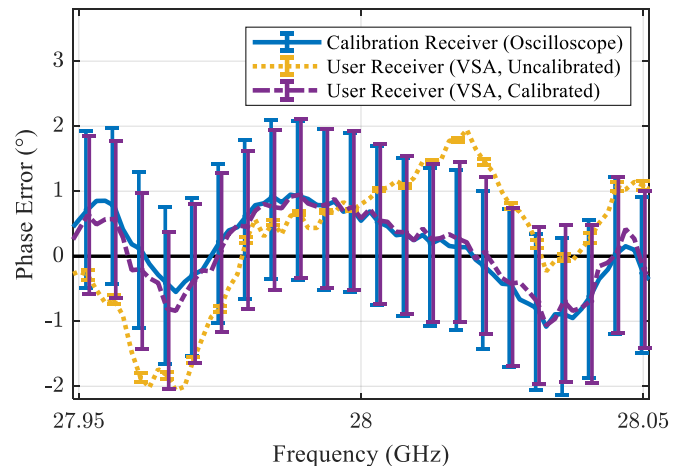


Fig. 6. The difference in relative phase (termed "phase error") of a predistorted calibration signal measured by a calibration receiver and an uncalibrated user receiver. The differences between the reference receiver and user receiver are used to derive the calibration coefficients for the user receiver to be used in an IEEE-1765 Measurement Comparison. Error bars indicate 95% confidence bounds based on uncertainty propagation and Monte-Carlo analysis.

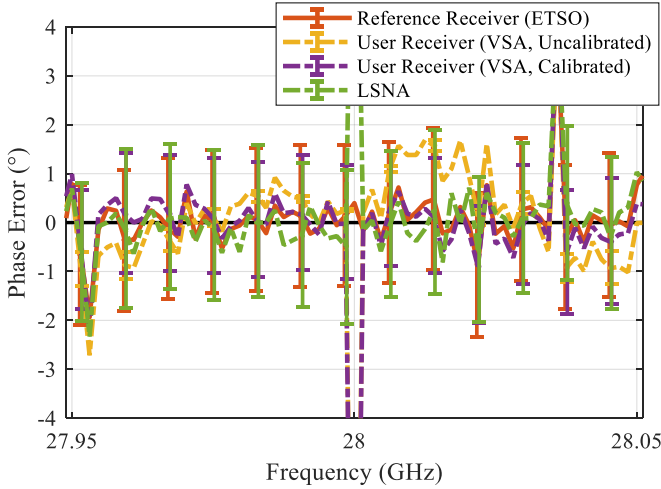


Fig. 7. Measurements of the same Test Waveform emanating from the same signal source by an ETSO Reference Receiver, a VSA User Receiver calibrated in post processing with the method described in the previous section, and a calibrated LSNA. Error bars indicate 95% confidence bounds based on uncertainty propagation and Monte-Carlo analysis.

selected was identical in modulation format and filter properties to the IEEE-1765 waveform but was produced at a lower sampling rate and with fewer symbols.

The multisine calibration waveform had a center frequency of 28 GHz, and a tone spacing of 1.5625 MHz, corresponding to a 640 ns envelope for the entire waveform. The main passband of the communication signal to be tested had a 133 MHz bandwidth (see the solid line in Fig. 4 (a)), and the calibration waveform was designed to with a 156.25 MHz bandwidth (dashed line in Fig. 4 (a)), in order to exceed the communication-signal bandwidth by 17% while still remaining within the maximum bandwidth of the VSA under test.

An important metric of interest for our calibration waveform is its PAPR, which measures the ratio of the peak power of the waveform versus its average power. The PAPR can be calculated from a signal's time-domain amplitude y by:

$$PAPR_{dB} = 10 \cdot \log_{10} \left(\frac{\max(y^2)}{y^2} \right). \quad (1)$$

Waveforms comprising sharp pulses typically have a high PAPR – much higher than those of communication waveforms. Such high-PAPR signals present a challenge for calibration for two reasons: first, they concentrate most of their signal power into a very short portion of the waveform's overall duration, and second, they produce wider swings of voltage on the signal generation and receiver hardware, increasing the potential for significant nonlinear effects. The cumulative effect of these factors is that high-PAPR waveforms can have a lower signal-to-noise and distortion (SINAD) ratio, resulting in increased uncertainties on the calibration.

The 101-tone multisine signal used in this demonstration was generated with a Schroeder relative phase relationship [23] and had a PAPR of 5.6 dB. For comparison, the PAPR of an ideal pulse, bandpass filtered to a 156.25 MHz bandwidth around 28 GHz is 23.0 dB. The PAPR of a QAM waveform depends on the exact arrangement of the QAM symbols within the waveform. The 64-QAM modulated signal used for EVM

calculations in this study had a PAPR of 8.0 dB, but a test of similar 64-QAM signals with random sequences of 64 symbols showed a range of PAPRs between 6.5 dB and 10.2 dB. For random selections of 16-QAM and 4-QAM waveforms, we find the PAPR ranges to be 6.1 dB – 9.6 dB, and 5.2 dB – 7.0 dB, respectively. Bearing in mind these PAPR ranges for different types of communication signals, the Schroeder waveform presents an adequate and familiar starting point as a calibration waveform.

We note that the calibration proposed herein is not capable of accounting for nonlinear effects such as intermodulation distortion, because the technique operates on an assumption of linear behavior in the receiver hardware. Because we do not calibrate out nonlinear effects in the receiver, we attempt to minimize them by operating the receiver with sufficiently low input power and gain as to present clipping or saturation of the internal hardware. In the case that the receiver's nonlinearities make it sensitive to small differences in PAPR, we caution that the receiver's configuration should first be adjusted before attempting this calibration. For this reason, we do not require that the PAPR of the calibration and communications signals match exactly. Rather, the important characteristics of our calibration waveform are that it contains spectral content which at least covers the bandwidth of the communication signal(s) of interest, that all frequency components have relatively the same amplitude, and that the duration of the calibration waveform matches that of the communication signal(s) of interest. Whereas the Schroeder waveform meets these requirements, the use of calibration and communication waveforms with tailored PAPR levels is an area for future study.

Both the calibration and communications waveforms are illustrated in Fig. 4. In cases where the calibration waveform has a different frequency grid from the communication signal, interpolation will be required to calculate the required calibration coefficients for the user receiver, which may introduce additional uncertainties.

B. Predistortion of the Calibration Waveform

Due to hardware nonidealities in the calibration source, the calibration signal will differ from the designed calibration waveform [1]. For example, the phase relationships of the waveform emitted from the calibration source may be different from those of the designed waveform, leading to a different PAPR than expected. To account for these nonidealities, the calibration waveform first predistorted, using the traceable calibration receiver to provide feedback to the predistortion process [6].

Our predistortion approach is an iterative process where a signal is generated by the AWG, measured by the calibrated oscilloscope, and compared to the ideal waveform. For an ideal waveform with frequency-domain complex coefficients given by X , we generate an initial waveform file for the signal source with $X_0 = X$, then measure the output of the source using the sampling oscilloscope. The calibrated output of the sampling oscilloscope is expressed as Y_0 . Then, the predistorted signal to apply to the AWG is calculated by:

$$X_1^{PreD} = \frac{X_0}{Y_0} X,$$

and if additional predistortion iterations are desired, the revised AWG waveform is calculated as:

$$X_{n+1}^{PreD} = \frac{X_n^{PreD}}{Y_n} X.$$

We use a qualitative metric to decide when to halt the predistortion process: when the difference between X_n^{PreD} and X_{n+1}^{PreD} is smaller than the noise in Y_n , the process is deemed satisfactory. In the experiment presented herein, the QAM and Schroeder waveforms were each predistorted for 9 iterations.

In the example here, a traceably calibrated equivalent-time sampling oscilloscope [24] was used as a calibration receiver to measure the predistorted calibration signal. The result of the calibration receiver measurement of the calibration waveform, called the calibrated signal, is stored in a calibration measurement file.

Impedance mismatch between a signal source and receiver can distort the amplitude and phase of the signal entering the receiver, resulting in inaccurate measurements. Therefore, impedance-mismatch correction is carried out as part of the calibration process. The importance of mismatch correction at mmWave frequencies is illustrated by the measurements of the reflection parameter S_{11} in Fig. 5, where we see significant changes in impedance over the bandwidth of interest. Uncertainties in impedance measurements are propagated to the calibration- and user-receiver measurements. A typical example of the mismatch terms and corresponding uncertainties calculated with the NIST Microwave Uncertainty Framework [25] is shown in Fig. 5.

For each waveform, 30 repeat measurements were performed with the sampling oscilloscope, and 200 repeat measurements were performed with the VSA. The oscilloscope measurements require approximately 10 minutes per acquisition (5 hours for 30 repeats), while the VSA measurements take less than 2 seconds to complete (4 minutes of data collection for 200 repeat measurements). The number of repeat measurements for the sampling oscilloscope was chosen based on past experience with the measurement system, and the number of VSA acquisitions was chosen to provide a reasonable data collection time. Repeat measurements were performed in a temperature-controlled lab environment, and the bending of the test-port cable when moved between the sampling oscilloscope and user-receiver was included as a source of measurement uncertainty. To correct for drift and time delay through transmission lines, measurement results were time aligned to each other [26]. Next, the time-aligned results were combined by averaging, and uncertainties based on the variance between repeat measurements were propagated along with measurement uncertainties such as those resulting from impedance mismatch, cable bending, and the oscilloscope impulse response. The phase error corresponding to the difference between the ideal Schroeder relative phases and the measured relative phases made with the calibration receiver are shown by the solid line in Fig. 6. Here we see a residual phase error of approximately $\pm 1^\circ$, with a 95% confidence interval of approximately 1° . The

error bars correspond to the modeled errors in the VNA calibration standards, oscilloscope measurements, and bending of the coaxial cable that carried the 28 GHz modulated waveform to the oscilloscope and to the VSA.

C. User-Receiver Measurement of the Calibration Signal

After measuring the predistorted calibration signal with the calibration receiver, the calibration signal source is connected to the user receiver. During this step, it is important to connect the user receiver at the same reference plane where calibration receiver measurements were taken, as shown in Fig. 1, or de-embed any additional adapters or cables in post-processing. It is also important to configure the VSA for a low-distortion measurement across the bandwidth of interest. For example, the configuration for a VSA should eliminate or minimize spectral leakage [27]. Additionally, the VSA gain and amplitude range should be selected to achieve the highest dynamic range before clipping or ADC overflow occurs. Depending on the particular VSA hardware, a number of configuration settings are available: preamplifiers, preselector filters, attenuation, and other options may be possible. The VSA calibration is valid only for a particular set of hardware and software configuration settings.

Measurements from the user receiver are also corrected for impedance mismatch between the user receiver (here the VSA) and the calibration source, determined with VNA measurements of both instruments (see Fig. 5). Additionally, the user-receiver measurements of the calibration waveform are time aligned to allow comparison of the phase measurements between the user receiver and the calibration receiver.

Many commercial receivers offer some form of “self-calibration” or “alignment” procedure wherein the instrument calibrates itself based on certain internal references. In our experiments, we performed this self-calibration procedure once, and then measured all waveforms (calibration and QAM test waveform) within 8 hours. For the purpose of this discussion, we consider this self-calibration process a part of the manufacturer-recommended application of the of instrument, but not a “calibration” in itself. Because this is purely an internal adjustment without reference to external calibration mechanisms, we term this an “uncalibrated” measurement. Any automated features of the instrument, such as automatic self-calibration or gain control, were disabled during this experiment to prevent unanticipated changes in the instrument’s state.

D. Calculation of Calibration Coefficients

Calibration coefficients that will be applied to subsequent measurements made with the VSA are calculated from the differences between calibration measurement ($x^{\text{cal data}}$) on the calibration receiver and measurements taken by the user receiver of the same calibration signal. Such differences can be seen in Fig. 6, which shows the phase error for the user-receiver measurement. The calibration coefficients may be calculated from complex Fourier coefficients as:

$$A_{\text{correction}} = x^{\text{cal data}} / x^{\text{user receiver measurement}} \quad (2)$$

Future measurements taken by the user receiver are corrected by these calibration coefficients in post processing to arrive at a calibrated user-receiver measurement result:

$$x^{calibrated} = x^{uncalibrated} A_{correction} \quad (3)$$

Uncertainties are propagated into the calibration coefficients as described above.

E. Calculation of Uncertainties

In the preceding plots of receiver measurements (Fig. 6 and Fig. 7), 95% confidence intervals were plotted along with the calibrated calibration-receiver measurements and the calibrated user-receiver measurements. These confidence intervals capture uncertainties associated with impedance measurements of the source, the user receiver, and the calibration receiver, including uncertainties in the calibration standards used. Additionally, uncertainties in the phase calibration are included, which incorporate oscilloscope measurements and oscilloscope calibration via an EOS-calibrated photodiode. Finally, the variances associated with the 200 repeat measurements of the user receiver and the 30 repeat measurements from calibration receiver are accounted for in these uncertainty values.

At each step in the calibration, the NIST Microwave Uncertainty Framework was used to propagate uncertainties. For this, a Monte-Carlo method is used to estimate the combined effect of multiple sources of uncertainty, which are propagated through the calibration. This numerical approach evaluates the uncertainty through nonlinear transformation, and accurately treats independent or interdependent sources of uncertainty. The sources of uncertainty considered include mechanical dimensions of the impedance calibration standards, calibration of the power sensor, and elements of the sampling oscilloscope calibration by means of the photodiode and electro-optical system [4]. Because the source, calibration receiver, reference receiver, and user receiver all have unique, frequency-dependent impedance, the reflection coefficient of each (receiver input and source output) is measured separately and taken into account during the calibration. Additionally, when measurements are averaged together, information on the statistical distribution of the measurements is retained for uncertainty estimation. More information on the automated propagation of uncertainties for microwave measurements can be found in [28][29].

III. IEEE-1765 MEASUREMENT COMPARISON

In the IEEE-1765-2022 measurement comparison methods described in [1], the reference laboratory measures and predistorts one of the IEEE-1765 Reference Waveforms. As discussed there, the resulting predistorted “Test Waveform” is not identical to the Reference Waveform due to residual distortion from the source and reference receiver [6]. The user-receiver measurement of the Test Waveform is calibrated in post processing for magnitude, phase, and impedance with the

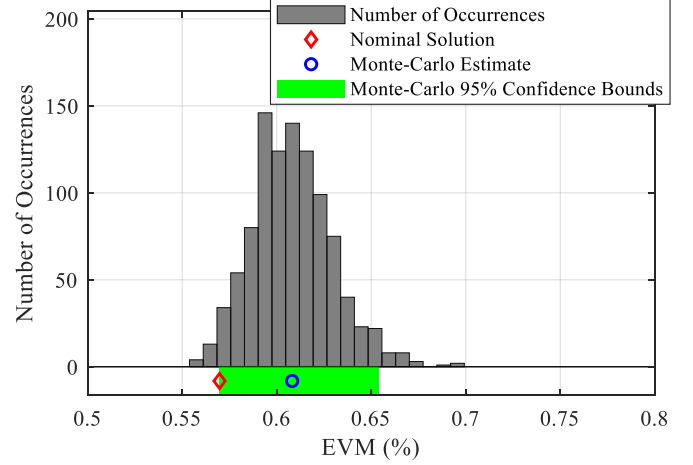


Fig. 8. Distribution of EVM values for QAM Test Waveform measured by reference receiver.

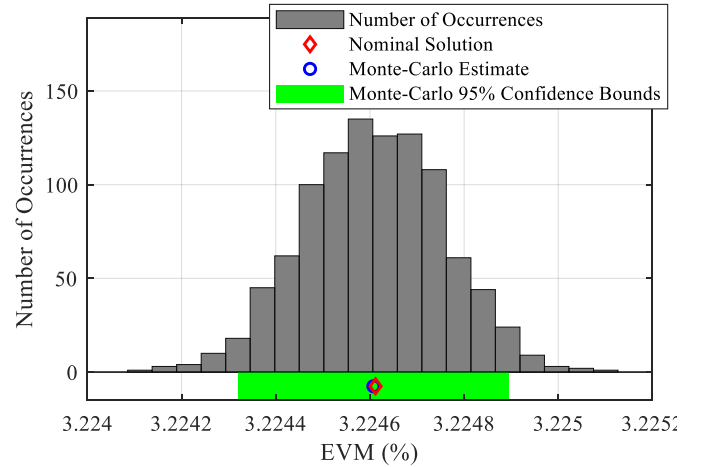


Fig. 9. EVM distribution for the measurement of QAM Test Waveform (same signal as in Fig.) using uncalibrated user receiver.

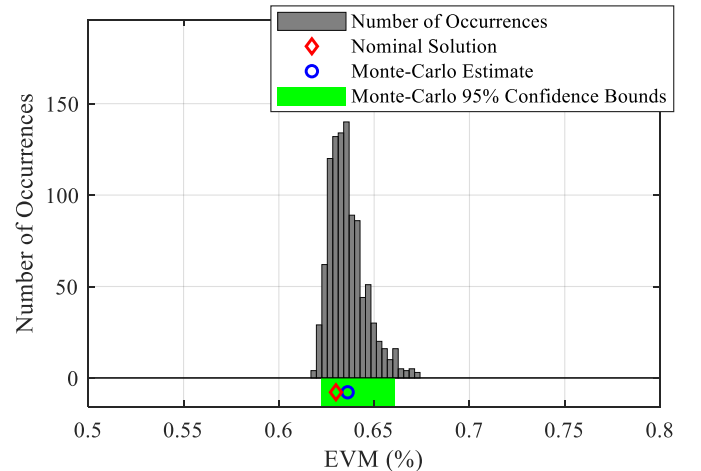


Fig. 10. EVM distribution for user-receiver measurement of QAM Test Waveform after calibration has been applied.

calibration coefficients derived in Section II and user-derived uncertainties are applied. The calibrated user-receiver waveform is then compared to the reference receiver’s measurement of the Test Waveform, which has its own uncertainty analysis. We use the calibration-comparison process, described in [1] Section 7.6 to compare measurements from the calibrated VSA with the reference-receiver measurements. The measurement comparison process is discussed in this section.

A. The Measurement Comparison Waveforms

The Test Waveform in our example is a 64-QAM modulated signal containing all 64 QAM symbols arranged in a random order. The signal is generated with a symbol rate of 100 MSymbol/s, and filtered through a root-raised cosine filter with a rolloff (beta) factor of 0.35. The bandwidth of this QAM signal is approximately 133 MHz, and it has a PAPR of 8.0 dB. The signal is generated at an IF frequency of 4.0 GHz using an AWG with a sampling rate of 60 GHz. The IF signal is combined with a 24 GHz LO to produce a QAM waveform at 28 GHz.

As mentioned in the introduction, the same receiver hardware was used for both the calibration and reference receivers, and the same signal-generation hardware was used in both steps. Thus, the calibrated VSA could not be expected to provide an EVM lower than that of the calibration receiver (the sampling oscilloscope). The “calibration” (Fig 1, steps 1 and 2) and “reference” (Fig 1, steps 2 and 3) phases are differentiated by the type of waveform measured: a multisine for the VSA calibration procedure (with complex calibration coefficients as output), and a 64-QAM modulated waveform for the measurement comparison procedure (with EVM as output).

User-receiver measurements were corrected in post processing with the calibration coefficients derived in the previous section. The corrected user- and reference-receiver measurements of phase error are plotted in Fig. 7.

Plotted error bars represent 95% uncertainty bounds based on uncertainties in impedance-match-corrected measurements. Components of uncertainty for each receiver were derived from S-parameter (mechanical), power, and phase calibrations, as well as cable bending and repeat measurements. Uncertainties were applied in the NIST Microwave Uncertainty Framework, maintaining correlations between components of uncertainty. Note that the error bars for both the sampling oscilloscope and VSA measurements are similar in magnitude. This is because the dominant uncertainty mechanism for these measurements corresponds to the phase reference (an equivalent-time sampling oscilloscope calibrated by comparison to electro-optic sampling system measurements of a photodiode [24]. This phase calibration was used in both measurements.

B. EVM Comparison

Values of EVM were derived from measurements of the 64-QAM communications Test Waveform, using the IEEE-1765 Baseline EVM Algorithm detailed in [1]. For each measurement, an EVM distribution was calculated using a Monte-Carlo approach as detailed in the next subsection.

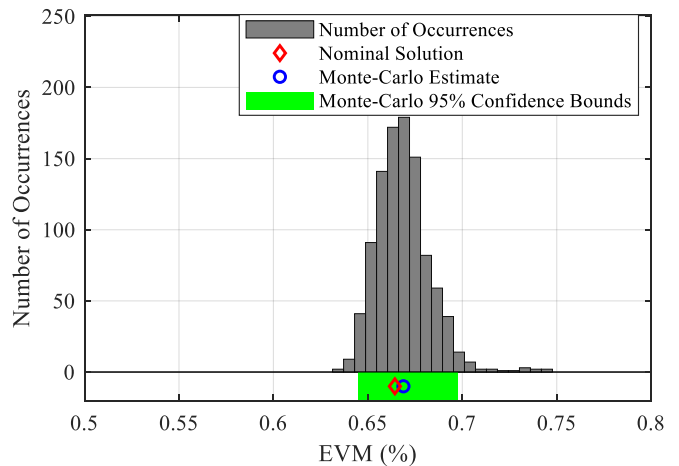


Fig. 11. EVM distribution for LSNA measurement of the QAM Test Waveform

The EVM for the reference receiver measurement of the predistorted 64-QAM waveform is plotted in Fig. 8. The mean value is 0.61%. The “nominal” EVM value plotted in Fig. 8 is an estimate of the EVM exclusive of the uncertainty mechanisms. The nominal EVM estimate falls below the mean of the Monte-Carlo EVM distribution, because distortion introduced due to non-idealities of the reference receiver are incorporated and minimized during the predistortion process. Thus, the nominal value of EVM derived from the reference receiver underestimates the “true” EVM of the waveform [1], [6]. Once the measurement uncertainties in the reference receiver are properly accounted for, including the systematic errors introduced by the VNA calibration standards and other systematic effects, the mean estimated value of EVM lies at the center of the Monte Carlo distribution of errors. Note that measurements of the predistorted waveform with receivers that did not perform the predistortion will not exhibit this effect. That is, the nominal and mean EVM values will be closer to each other, as seen by the VSA measurements.

In Fig. 9, the EVM distribution is plotted for measurement from the uncalibrated user receiver, where only the “front panel” VSA calibration has been applied. The mean value of EVM for this case is 3.22%. For this plot, only uncertainties due to repeat measurements are considered, as uncertainty in amplitude, phase, and impedance mismatch are not introduced until the calibration step. As a result, the width of the 95% confidence interval is small (<0.01%) as compared that of the reference-receiver measurements (0.08%). Additionally, we see that the nominal and Monte-Carlo estimated values are in close agreement, as discussed above.

When the calibration coefficients derived in Section II are applied to the VSA measurements, the mean estimated EVM is reduced to 0.636%, as shown in Fig. 10. The width of the uncertainty distribution for this case is increased as compared to that of Fig. 9 due to incorporation of uncertainties during the receiver calibration.

IEEE-1765-2022 utilizes a calibration-comparison error metric (E_n) to compare the user-receiver measurements with

those from the reference receiver. Given an EVM estimated from the user-receiver (x), EVM estimated from the reference-receiver (X), and expanded uncertainties from the user- and reference-receivers (U_{lab} and U_{ref}), the error metric E_n is calculated by

$$E_n = \frac{x - X}{\sqrt{U_{lab}^2 + U_{ref}^2}}. \quad (3)$$

When $|E_n| < 1$, the measurements are deemed adequately comparable. This function and the $|E_n| < 1$ criterion are specified in the ISO/IEC 17043 as the recommended method for evaluating agreement between two quantities [30].

As noted above, because the same sampling oscilloscope was used as calibration and reference receiver, the best agreement that can be obtained is when the VSA-measured EVM agrees with the reference-receiver-measured EVM. This is confirmed by calculation of the error metric, E_n , where $|E_n| = 0.30$ for comparison between the user-receiver (calibrated VSA) and the reference-receiver. In contrast, the error metric for the uncalibrated VSA relative to the reference-receiver measurement is where $|E_n| = 30.95$. The agreement between the reference and user receiver values of EVM both illustrates the utility of the IEEE-1765 measurement comparison approach and confirms the improvement provided by calibration of the VSA.

C. Comparison to LSNA Measurement

To provide an additional example of the IEEE-1765 measurement-comparison approach, a calibrated large-signal network analyzer (LSNA) was used to measure the same 64-QAM Test Waveform that was measured by the user receiver (VSA) and reference receiver (sampling oscilloscope). The LSNA was calibrated for impedance mismatch, magnitude, and phase using the techniques described in [31][32].

In the LSNA measurement setup, the modulated-signal source replaces the LSNA's internal source, and the Test Waveform is sent through the instrument's directional couplers before emerging from the front-panel test ports. This enables simultaneous measurement of the forward ("a") and reflected ("b") waves from the LSNA's test ports and obviates the need for a separate impedance mismatch measurement of the user receiver. A second RF channel from the signal source is used to provide a phase reference to the LSNA, allowing for phase-coherent measurements as the receivers of the LSNA step from frequency to frequency. We extend the work of [19] in two ways. First, the LSNA's phase measurements are calibrated by measuring a multisine waveform on the LSNA and on a calibrated sampling oscilloscope, enabling full measurement traceability in terms of magnitude, phase, and power. Second, EVM is calculated using the open-source IEEE-1765 algorithm, with measurement uncertainties propagated through the NIST Microwave Uncertainty Framework. This enables the full physical models of the uncertainty mechanisms, and their associated correlations, to be propagated fully into the reported EVM values. In Fig. 7, the phase measurement of the LSNA is plotted alongside measurements from the reference- and user

receivers.

EVM results for the LSNA measurement of the Test Waveform are plotted in Fig. 11. The LSNA's EVM result of 0.67%, with a confidence interval of 0.053%, was found to agree with the reference receiver's result with $|E_n| = 0.61$ from equation (3). Whereas the distribution of the LSNA's EVM values does agree with those of the reference and user receivers, we note that it is higher than that of the user receiver (VSA). This is believed to be due to multiplexing between the LSNA's measurement receivers, which occurs under some configurations of the instrument when individual IF receivers are shared between multiple receive channels, incurring a time delay between measurement of the signal and phase reference – future work involves mitigating this phase noise by changing the LSNA configuration.

IV. CONCLUSIONS

The IEEE-1765-2022 standard describes several techniques for the estimation of errors introduced by measurement hardware in EVM derived from the measurement of modulated waveforms. In the IEEE-1765 measurement comparison techniques, waveform measurements from a user's receiver are compared to measurements of the same waveform using a calibrated reference receiver. Calibration of the user's receiver is necessary to provide uncertainty information in EVM results. We illustrated this approach with a system-level calibration for a mmWave VSA, which enabled the propagation of measurement uncertainties from transfer standards to the final EVM estimate. Our results demonstrated a significant and quantifiable improvement in the VSA's measurement of EVM after the application of complex-valued calibration coefficients.

Whereas the calibrations described herein were for an instrument of relatively low bandwidth (160 MHz), contemporary VSA instruments are capable of measurements with more than 1 GHz bandwidth at frequencies above 100 GHz. The techniques described herein are limited mainly by the traceable calibration of the sampling oscilloscope, which is limited to 110 GHz at present [4]. Contemporary developments in S-parameter measurement to above 1 THz [33], and electro-optic phase references above 110 GHz [34] will be enabling technologies for VSA calibrations between 100 GHz and 1 THz.

REFERENCES

- [1] IEEE Standards Association, "1765-2022 IEEE Recommended Practice for Estimating the Uncertainty in Error Vector Magnitude of Measured Digitally Modulated Signals for Wireless Communications," Nov. 2022.
- [2] D. Williams, P. Hale and K. A. Remley, "The Sampling Oscilloscope as a Microwave Instrument," in *IEEE Microwave Magazine*, vol. 8, no. 4, pp. 59-68, Aug. 2007, doi: 10.1109/MMW.2007.383954.
- [3] D. F. Williams, T. S. Clement, P. D. Hale and A. Dienstfrey, "Terminology for high-speed sampling-oscilloscope calibration," *2006 68th ARFTG Conference: Microwave Measurement*, Broomfield, CO, USA, 2006, pp. 1-6, doi: 10.1109/ARFTG.2006.8361647.
- [4] T. S. Clement, P. D. Hale, D. F. Williams, C. M. Wang, A. Dienstfrey and D. A. Keenan, "Calibration of sampling oscilloscopes with high-speed photodiodes," in *IEEE Transactions on Microwave Theory and*

- Techniques*, vol. 54, no. 8, pp. 3173-3181, Aug. 2006, doi: 10.1109/TMTT.2006.879135
- [5] P. D. Hale, C. M. Wang, D. F. Williams, K. A. Remley and J. D. Wepman, "Compensation of Random and Systematic Timing Errors in Sampling Oscilloscopes," in *IEEE Transactions on Instrumentation and Measurement*, vol. 55, no. 6, pp. 2146-2154, Dec. 2006, doi: 10.1109/TIM.2006.880270
- [6] K. A. Remley, D. F. Williams, P. D. Hale, C. Wang, J. Jargon and Y. Park, "Millimeter-Wave Modulated-Signal and Error-Vector-Magnitude Measurement With Uncertainty," in *IEEE Transactions on Microwave Theory and Techniques*, vol. 63, no. 5, pp. 1710-1720, May 2015, doi: 10.1109/TMTT.2015.2416180.
- [7] P. Manurkar, C. P. Silva, J. Kast, R. D. Horansky, D. F. Williams and K. A. Remley, "Reference Measurements of Error Vector Magnitude," *2022 IEEE/MTT-S International Microwave Symposium - IMS 2022*, Denver, CO, USA, 2022, pp. 1026-1029, doi: 10.1109/IMS37962.2022.9865278.
- [8] P. D. Hale, K. A. Remley, D. F. Williams, J. A. Jargon and C. M. J. Wang, "A compact millimeter-wave comb generator for calibrating broadband vector receivers," *2015 85th Microwave Measurement Conference (ARFTG)*, 2015, pp. 1-4, doi: 10.1109/ARFTG.2015.7162894.
- [9] M. Vanden Bossche, F. Verbeyst and A. Samant, "Traceable phase calibration of a wide-bandwidth microwave Vector Signal Analyzer," *2015 IEEE MTT-S International Microwave Symposium*, 2015, pp. 1-4, doi: 10.1109/MWSYM.2015.7167125.
- [10] D. A. Humphreys, M. Hudlička and I. Fatadin, "Calibration of Wideband Digital Real-Time Oscilloscopes," in *IEEE Transactions on Instrumentation and Measurement*, vol. 64, no. 6, pp. 1716-1725, June 2015, doi: 10.1109/TIM.2015.2407471.
- [11] H. C. Reader, D. F. Williams, P. D. Hale and T. S. Clement, "Comb-Generator Characterization," in *IEEE Transactions on Microwave Theory and Techniques*, vol. 56, no. 2, pp. 515-521, Feb. 2008, doi: 10.1109/TMTT.2007.914630.
- [12] C. Cho, H. Koo, J. Kwon and J. Lee, "Uncertainty Analysis for Characterization of a Commercial Real-Time Oscilloscope Using a Calibrated Pulse Standard," in *IEEE Access*, vol. 7, pp. 159724-159730, 2019, doi: 10.1109/ACCESS.2019.2950683.
- [13] D. F. Williams, P. D. Hale, T. S. Clement and J. M. Morgan, "Calibrating electro-optic sampling systems," *2001 IEEE MTT-S International Microwave Symposium Digest (Cat. No.01CH37157)*, 2001, pp. 1527-1530 vol.3, doi: 10.1109/MWSYM.2001.967193.
- [14] M. Hudlicka, "Laboratory system for a traceable measurement of error vector magnitude," *2009 European Microwave Conference (EuMC)*, 2009, pp. 934-937, doi: 10.23919/EUMC.2009.5296163.
- [15] D. A. Humphreys, M. R. Harper and M. Salter, "Traceable calibration of Vector Signal Analyzers," *75th ARFTG Microwave Measurement Conference*, 2010, pp. 1-4, doi: 10.1109/ARFTG.2010.5496315.
- [16] F. Zhou, R. Zhang, D. Mu, K. Cheng, Y. -c. Xu and Y. -g. Gao, "Method for calibration vector signal analyzer based on baseband waveform design," *83rd ARFTG Microwave Measurement Conference*, 2014, pp. 1-14, doi: 10.1109/ARFTG.2014.6899519.
- [17] C. M. J. Wang, P. D. Hale, J. A. Jargon, D. F. Williams and K. A. Remley, "Sequential Estimation of Timebase Corrections for an Arbitrarily Long Waveform," in *IEEE Transactions on Instrumentation and Measurement*, vol. 61, no. 10, pp. 2689-2694, Oct. 2012, doi: 10.1109/TIM.2012.2193692
- [18] P. D. Hale, D. F. Williams and A. Dienstfrey, "Waveform metrology: signal measurements in a modulated world." *Metrologia* 55, no. 5. 2018
- [19] Y. Zhang *et al.*, "Evaluating EVM Performance in Millimeter Wave OTA Test using Digitally Modulated Stimuli with Pre distortion and a NVNA Test Bench," in *IEEE Transactions on Antennas and Propagation*, doi: 10.1109/TAP.2024.3438352
- [20] N. B. Carvalho, K. A. Remley, D. Schreurs and K. G. Gard, "Multisine signals for wireless system test and design [Application Notes]," in *IEEE Microwave Magazine*, vol. 9, no. 3, pp. 122-138, June 2008, doi: 10.1109/MMM.2008.919938.
- [21] K. A. Remley, "Multisine excitation for ACPR measurements," *IEEE MTT-S International Microwave Symposium Digest*, 2003, 2003, pp. 2141-2144 vol.3, doi: 10.1109/MWSYM.2003.1210586.
- [22] J. C. Pedro and N. B. Carvalho, "Designing multisine excitations for nonlinear model testing," in *IEEE Transactions on Microwave Theory and Techniques*, vol. 53, no. 1, pp. 45-54, Jan. 2005, doi: 10.1109/TMTT.2004.839340.
- [23] M. Schroeder, "Synthesis of low-peak-factor signals and binary sequences with low autocorrelation (Corresp.)," in *IEEE Transactions on Information Theory*, vol. 16, no. 1, pp. 85-89, January 1970, doi: 10.1109/TIT.1970.1054411.
- [24] T. S. Clement, P. D. Hale, D. F. Williams, C. M. Wang, A. Dienstfrey and D. A. Keenan, "Calibration of sampling oscilloscopes with high-speed photodiodes," in *IEEE Transactions on Microwave Theory and Techniques*, vol. 54, no. 8, pp. 3173-3181, Aug. 2006, doi: 10.1109/TMTT.2006.879135.
- [25] *NIST Microwave Uncertainty Framework*. (2011). National Institute of Standards and Technology, <http://www.nist.gov/ct/rf-technology/related-software.cfm>. [Online]. Available: <http://www.nist.gov/ct/rf-technology/related-software.cfm>
- [26] K. A. Remley, D. F. Williams, D. M. M. -. Schreurs, G. Loglio and A. Cidronali, "Phase detrending for measured multisine signals," *61st ARFTG Conference Digest*, Spring 2003., Philadelphia, PA, USA, 2003, pp. 73-83, doi: 10.1109/ARFTGS.2003.1216870.
- [27] M.D. McKinley, K.A. Remley, M. Myslinski, and J.S. Kenney, "Eliminating FFT artifacts in vector signal analyzer spectra". *Microwave Journal*, vol. 49 no.10 October 2006
- [28] D. F. Williams, NIST Microwave Uncertainty Framework, Beta Version. NIST, Boulder, CO, USA, Jun. 2014. [Online]. Available: <http://www.nist.gov/pml/electromagnetics/related-software.cfm>
- [29] J. A. Jargon, D. F. Williams, T. M. Wallis, D. X. LeGolvan, and P. D. Hale, "Establishing traceability of an electronic calibration unit using the NIST Microwave Uncertainty Framework," in *79th ARFTG Conf. Dig.*, Montreal, QC, Canada, Jun. 2012, pp. 32-36s
- [30] *ISO/IEC 17043:2010, Conformity assessment — General requirements for proficiency testing*, Feb. 30 2010.
- [31] A. Sanders, D. F. Williams, J. M. Kast, K. A. Remley and R. D. Horansky, "Large-Signal-Network-Analyzer Phase Calibration on an Arbitrary Grid," *2019 IEEE MTT-S International Microwave Symposium (IMS)*, 2019, pp. 1391-1394, doi: 10.1109/MWSYM.2019.8700829.
- [32] J. M. Kast, P. Manurkar, K. A. Remley, R. Horansky and D. F. Williams, "Traceable mm Wave Modulated-Signal Measurements for OTA Test," *2022 99th ARFTG Microwave Measurement Conference (ARFTG)*, Denver, CO, USA, 2022, pp. 1-4, doi: 10.1109/ARFTG54656.2022.9896560.
- [33] J. Cheron *et al.*, "A 0.1 GHz to 1.1 THz Inverted Grounded-CPW mTRL Calibration Kit Characterization in an InP HBT Process," *2024 IEEE Wireless and Microwave Technology Conference (WAMICON)*, Clearwater, FL, USA, 2024, pp. 1-4, doi: 10.1109/WAMICON60123.2024.10522868.
- [34] B. T. Bosworth, A. Osella, T. Ishibashi, A. D. Feldman and N. D. Orloff, "Optoelectronic primary standards for phase references to sub-THz frequencies," *OPTO*, San Francisco, CA, USA, 2025, doi: <https://doi.org/10.1117/12.3041446>



Joshua M. Kast (Member, IEEE) received the Ph.D. in electrical engineering from the Colorado School of Mines, Golden, CO, USA, in 2022. He joined the NIST Communications Technology Laboratory as a graduate student associate in 2017, and as an NRC postdoctoral associate in 2023. His research includes finite-difference methods for electromagnetic simulation, nonlinear vector network analyzer applications, X-Parameter device characterization, timing uncertainty, modulated signal characterization, synthetic-aperture applications, and electro-optic measurements. He is currently with the High-Speed Waveform Metrology group at NIST.



Paritosh Manurkar (Senior Member, IEEE) received the Ph.D. degree in electrical engineering from Northwestern University, Evanston, IL, USA, in 2016. He is currently a Senior Research Associate at the University of Colorado (CU) at Boulder, Boulder, CO, USA and

performs his research at the National Institute of Standards and Technology (NIST), Boulder, through a CU-NIST Partnership. He is currently working with the Shared Spectrum Metrology Group in the RF noise measurement project. He has previously worked on development of precision, calibrated, millimeter-wave modulated-signal sources, performing traceable over-the-air measurements, channel sounding, time and frequency transfer between optical clocks, development of fully self-referenced fiber frequency combs, nonlinear optics experiments using shaped pulses, fabrication of infrared detectors, and semiconductor engineering. He is actively involved in standards development as the Chair of the IEEE P1765 Working Group, a member of the IEEE Synthetic Aperture Technical Working Group (SA-TWG), and a member of the IEEE Microwave Theory and Technology Society's (MTT-S) Standards Committee (SC).



Kate A. Remley (S'92-M'99-SM'06-F'13) was born in Ann Arbor, MI. She received the Ph.D. degree in Electrical and Computer Engineering from Oregon State University, Corvallis, in 1999.

From 1983 to 1992, she was a Broadcast Engineer in Eugene, OR, serving as Chief Engineer of an AM/FM broadcast station from 1989-1991. In 1999, she joined the RF Technology Division of the National Institute of Standards and Technology (NIST), Boulder, CO, as an Electronics Engineer. She was the Leader of the Metrology for Wireless Systems Project at NIST from 2003 to 2022, where her research activities included development of calibrated measurements for microwave and millimeter-wave wireless systems and standardized over-the-air test methods for the wireless industry and public-safety sectors. In July 2022, she retired from NIST.

Dr. Remley is a Fellow of the IEEE and was the recipient of the Department of Commerce Bronze and Silver Medals, an ARFTG Best Paper Award, the NIST Schlichter Award, and is a member of the Oregon State University Academy of Distinguished Engineers. She was the Chair of the MTT-11 Technical Committee on Microwave Measurements (2008-2010), the Editor-in-Chief of IEEE Microwave Magazine (2009-2011), and Chair of the MTT Fellow Evaluating Committee (2017-2018). She was a Distinguished Lecturer for the IEEE Electromagnetic Compatibility Society (2016-2017) and was the co-Technical Program Chair for the IEEE International Microwave Symposium IMS2022.



Dylan Williams (Life Fellow, IEEE) received a Ph.D. in Electrical Engineering from the University of California, Berkeley in 1986. He joined the Electromagnetic Fields Division of the National Institute of Standards and Technology in 1989 where he develops electrical waveform and microwave metrology. He has published over 140

technical papers and is a Fellow of the IEEE. He is the recipient of the Department of Commerce Bronze and Silver Medals, the Astin Measurement Science Award, two Electrical Engineering Laboratory's Outstanding Paper Awards, three Automatic RF Techniques Group (ARFTG) Best Paper Awards, the ARFTG Automated Measurements Technology Award, the IEEE Morris E. Leeds Award, the European Microwave Prize and the 2013 IEEE Joseph F. Keithley Award. Dylan also served as Editor of the IEEE Transactions on Microwave Theory and Techniques from 2006 to 2010, as the Executive Editor of the IEEE Transactions on Terahertz Science and Technology, and as the 2017 President of the IEEE Microwave Theory and Techniques Society.



Robert D. Horansky Robert D. Horansky received the B.A. degree in chemistry and the Ph.D. degree in physics from the University of Colorado, Boulder, CO, USA, in 1999 and 2005, respectively. His thesis work focused on low-noise dielectric measurements on novel materials in molecular electronics. Since 2005, he

has been with the National Institute of Standards and Technology (NIST), Boulder, CO, USA, where he started out developing the highest resolving power energy dispersive sensor to date. He then went on to develop metrology techniques for single photon sensors in nuclear radiation and optical power measurements. In 2015, he joined the Metrology for Wireless Systems Project in the Communications Technology Laboratory, NIST developing calibrations and traceability for millimeter-wave wireless systems and reverberation-chamber measurements for cellular applications. He is the Secretary of the IEEE P1765 Standards Working Group on Uncertainty for EVM, and the winner of two Department of Commerce Medals for research in LTE Factor Screening and Novel Single Photon Detectors.